Journal of Organometallic Chemistry, 250 (1983) 345–371
Elsevier Sequoia S.A., Lausanne – Printed in The Netherlands

LIGAND EXCHANGE OF METAL CARBONYLS BY CHAIN MECHANISMS. ELECTROCHEMICAL KINETICS OF ELECTRON TRANSFER CATALYSIS

J.W. HERSHBERGER, C. AMATORE and J.K. KOCHI

Department of Chemistry, Indiana University, Bloomington, Indiana 47405 (U.S.A.)

(Received November 3rd, 1982)

Summary

The metal carbonyl derivatives $LM(CO)_n$ of manganese, rhenium, molybdenum and tungsten undergo facile ligand substitution by an electrode-mediated process. Phosphine, pyridine and isocyanide substitutions are shown to be chain reactions by coulometric analysis and by cyclic voltammetry of the metal carbonyl solutions containing the added nucleophiles ***L***. Reversible electrochemical parameters can be obtained for both $LM(CO)_n$ and the substitution product $\boldsymbol{L}M(CO)_n$. These allow the digital simulation of the cyclic voltammograms by Feldberg's method, which provides a detailed analysis of the kinetics of the electrocatalytic mechanism for ligand substitution. Generally, the radical cation $LM(CO)_n^+$ produced initially at the anode undergoes rapid exchange with ***L*** to afford the cationic substituted species $\boldsymbol{L}M(CO)_n^+$. This step is followed by electron transfer with the reactant $LM(CO)_n$ to yield the substitution product $\boldsymbol{L}M(CO)_n$ and regenerate the radical cation $LM(CO)_n^+$, which completes the chain propagation sequence. Multiple repetition of this cycle is indicated by the high current efficiencies which are obtainable. The second order rate constants for the ligand exchange of the 17-electron radical cations $LM(CO)_n^+$ with added ***L*** are evaluated, and found to be more than 10^6 times larger than that for the neutral, diamagnetic precursor $LM(CO)_n$. The radical cations $\boldsymbol{L}M(CO)_n^+$ also react readily with phosphine and alkyl isocyanide nucleophiles, leading to a characteristic distortion of the CV waves. Digital simulation of such cyclic voltammograms allows the kinetics of these processes, particularly the redox catalysis in the oxidation of phosphines by $LM(CO)_n^+$, to be evaluated quantitatively. The enhanced reactivity of the 17-electron radical cations $LM(CO)_n^+$ is discussed in relationship to recent reports of the substitution lability in other 17- and 19-electron metal carbonyls.

Introduction

Ligand exchange in metal carbonyls and their derivatives has received extensive mechanistic scrutiny [1–3]. The generally accepted mechanisms for the displacement of the ligand L from a series of metal carbonyls $LM(CO)_n$ by added nucleophiles ***L***

0022-328X/83/$03.00

such as amines, phosphines, etc., involve diamagnetic intermediates, generally with 16- and 18-electron configurations, in competing dissociative and associative

$$LM(CO)_n + L \rightarrow LM(CO)_n + L \quad (1)$$

processes [3,4]. However, there are recent reports of ligand substitution in 17-electron metal carbonyls which proceed via a purely associative process [5,6]. Furthermore, we have demonstrated that the facile substitution of nitrogen-centered ligands like acetonitrile and pyridine in such molybdenum, tungsten and manganese carbonyls as $LM(CO)_n$ = *fac*-$(MeCN)_3W(CO)_3$, *cis*-$(py)_2Mo(CO)_4$, and $(\eta^5$-$C_5H_4Me)Mn(CO)_2(py)$ by added phosphines and isonitriles is actually a chain process which proceeds via the 17-electron radical cations, $(py)_2Mo(CO)_4^+$, and $(MeCN)_3W(CO)_3^+$, $(\eta^5$-$C_5H_4Me)Mn(CO)_2(py)^+$, respectively [7,8].

Electrochemical techniques are ideally suited for the study of the radical cations of metal carbonyls since the electrode potential can be tuned to the redox potential of the diamagnetic precursor $LM(CO)_n$. Thus the chain process for ligand substitution can be induced (i.e., initiated) by the anodic generation of the carbonylmetal radical at the electrode [E]

$$LM(CO)_n \overset{[\vec{E}]}{\rightarrow} LM(CO)_n^+ \quad (2)$$

The kinetic lability of this carbonylmetal radical is central to the efficiency of the chain process, and it is included as eq.3 for the catalytic cycle in Scheme 1.

SCHEME 1

$$LM(CO)_n^+ + L \rightarrow LM(CO)_n^+ + L \quad (3)$$

$$LM(CO)_n^+ + LM(CO)_n \rightarrow LM(CO)_n + LM(CO)_n^+ \quad (4)$$

$$LM(CO)_n^+ \overset{[\bar{E}]}{\rightarrow} LM(CO)_n \quad (5)$$

The steps included in eqs. 2 and 5 are heterogeneous electron transfer processes occurring at the electrode, and those in eqs. 3 and 4 are homogeneous chain propagation reactions taking place in solution. Scheme 1 is characteristic of an electrochemical $\vec{E}C\bar{E}$ mechanism *, and the extent to which the cycle is repeated represents an electrocatalytic phenomenon. It should be noted that metal carbonyls such as *fac*-$(MeCN)_3W(CO)_3$ can be involved in multiple substitution of the three acetonitrile ligands by a series of sequential steps [7].

In this study we wish to show how the electrocatalytic method for ligand substitution can be extended to the rhenium complex $(\eta^5$-$C_5H_5)Re(CO)_2(py)$, and to examine further the use of bulk and transient electrochemical methods for the quantitative study of ligand substitution. We are concerned particularly with the kinetic analysis of the catalytic process for ligand substitution by digital simulation of the cyclic voltammograms.

Results

Coulometric evidence for electrocatalysis of ligand exchange

Electrocatalysis of ligand exchange is best illustrated by examining the effect of

* ECE refers to an initial electrode process followed by a homogeneous chemical reaction to form a second electroactive species.

an extremely small anodic current upon solutions of metal carbonyls containing added nucleophiles. Several representative systems are included in Table 1. The electrocatalytic process was conveniently monitored by following the changes in the infrared spectra arising from the disappearance and appearance of the characteristic carbonyl stretching frequencies of the reactant $LM(CO)_n$ and of the product $\boldsymbol{L}M(CO)_n$, respectively. Complete conversion required substantially less than 1 Faraday of charge per mole of metal carbonyl. The current efficiency for ligand substitution is given in column 6 of Table 1 by the ratio m/n, which is the electrochemical equivalent of a catalytic turnover number since it represents the moles m of $LMn(CO)_n$ consumed per Faraday n of charge passed through the solution. Values of m/n exceeding 1000 have been observed for the electrocatalytic substitution of the acetonitrile ligand in $(\eta^5\text{-}C_5H_4Me)Mn(CO)_2(NCMe)$ by the phosphines PPh_3 and $P(Me)Ph_2$. In each case, the substitution product of electrocatalysis $\boldsymbol{L}M(CO)_n$ was isolated and compared with that of an authentic sample prepared by an independent procedure. Since the amount of $LM(CO)_n$ destroyed by electrolysis was negligible, high yields of the substitution product were generally obtained.

It is important to emphasize that ligand substitution in these systems (particularly entries 1, 3, 4 and 5 in Table 1) did not occur for periods of several hours in the absence of an electrical current provided pure materials were employed. Thus the wholly thermal process for ligand substitution in eq.1 was not observed when the solutions were rigorously deoxygenated and the starting metal carbonyls were free of impurities. Moreover, we found that the latter were best removed by applying a slight cathodic current through the solution (at a potential where $LM(CO)_n$ was not itself reduced) prior to the introduction of the nucleophile $\boldsymbol{L}$. Actinic irradiation by adventitious roomlight was avoided owing to the possibility of a photoinduced substitution which has been previously established for various Group VIB and VIIB metal carbonyls [9–13].

There are several results in Table 1 which merit special attention. For the first entry, *cis*-$(py)_2Mo(CO)_4$, the possibility exists for either one or both pyridine ligands to be replaced by t-butyl isocyanide. Indeed, we only observed the disubstitution product *cis*-$(t\text{-}BuNC)_2Mo(CO)_4$ which was unambiguously identified by comparison with an authentic sample.

$$\begin{matrix}py\\py\end{matrix}\!\!>\!Mo(CO)_4 + 2\ t\text{-}BuNC \xrightarrow{[E]} \begin{matrix}t\text{-}BuNC\\t\text{-}BuNC\end{matrix}\!\!>\!Mo(CO)_4 + 2\ py \qquad (6)$$

A contrasting behavior was observed with the tungsten analog *cis*-$(py)_2W(CO)_4$, in which the presence of excess PPh_3 led only to the mono-substitution product under similar conditions [7]. The second entry in Table 1 represents a metal carbonyl which is by itself somewhat labile, and a slow thermal substitution of the tetrahydrofuran (THF) ligand was observed.

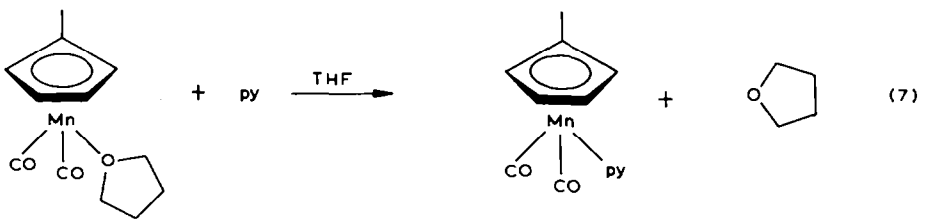

(7)

TABLE 1

ELECTROCATALYSIS OF LIGAND EXCHANGE OF REPRESENTATIVE METAL CARBONYLS BY ADDED NUCLEOPHILES *L* [a]

$LM(CO)_n$ (mmol)	*L* (mmol)	Solvent	Current (mA)	*T* (°C)	Current efficiency (m/n) [b]	$LM(CO)_n$ yield (%)
1. *cis*-$(CO)_4Mo(py)_2$ (0.14)	Me_3CNC (0.55)	MeCN	1.0	0	5.3	80 [d,e]
2. $(\eta^5$-$C_5H_4Me)Mn(CO)_2(THF)$ (0.23)	(py) (0.30)	THF	1.0	0	91	> 95 [g]
3. $(\eta^5$-$C_5H_4Me)Mn(CO)_2(MeCN)$ (0.12)	$P(OMe)Ph_2$ (0.14)	MeCN	0.10	22	833	> 95 [g]
4. $(\eta^5$-$C_5H_4Me)Mn(CO)_2(py)$ (0.12)	Me_3CNC (0.15)	Me_2CO	0.10	22	64	> 95 [f,g]
5. $(\eta^5$-$C_5H_5)Re(CO)_2(py)$ (0.067)	PPh_3 (0.094)	Me_2CO	0.50	22	5.6	86 [h]

[a] Controlled-current (galvanostatic)oxidations were performed in 12 ml of solvent with Pt gauze anode. In acetone and MeCN the supporting electrolyte was 0.1 *M* TEAP, and in THF it was 0.1 *M* TBAP. [b] The current efficiency, m/n, defined as the moles of starting material (m) consumed divided by the Faradays of charge (n) passed through the solution. [c] Product yield determined by quantitative IR spectrophotometry of the anolyte. [d] The product is *cis*-$(CO)_4Mo(CNCMe_3)_2$. [e] Ref 7. [f] Ref 8a. [g] Ref 8b. [h] This work.

However, the application of a 1 mA current led to an accelerated substitution by a factor of about 10-fold with a current efficiency approaching 10^2, despite the use of THF as the solvent itself. The fifth entry emphasizes that the rhenium carbonyl $(\eta^5\text{-}C_5H_5)Re(CO)_2(py)$ undergoes ligand substitution much like its manganese counterpart (entries 3 and 4), although with somewhat diminished current efficiency.

$$\begin{array}{l} CpRe(CO)_2 \\ \quad | \\ \quad py \end{array} + PPh_3 \xrightarrow{[E]} \begin{array}{l} CpRe(CO)_2 \\ \quad | \\ \quad PPh_3 \end{array} + py \qquad (8)$$

Nonetheless, the substitution product with $L = PPh_3$ can be obtained in high yields.

Cyclic voltammetric studies of electrocatalysis

In order to probe the origin of electrocatalysis in ligand substitution, we examined the transient electrochemical behaviour of metal carbonyls, both in the absence and presence of added nucleophiles *L*. The cyclic voltammetry (CV) was carried out at a stationary platinum microelectrode in acetonitrile, acetone or tetrahydrofuran solutions containing 0.1 *M* tetraalkylammonium perchlorate as supporting electrolytes. The cyclic voltammetric studies were performed on solutions which were deoxygenated with a stream of argon and maintained in subdued light. Voltage sweeps did not perturb the bulk properties of the solution, as evidenced by the reproducibility of the cyclic voltammograms, even after numerous scans. Thus the extent of net ligand substitution was negligible over the course of the CV experiments.

The CV data for the various metal carbonyls examined in this study are summarized in Table 2.

In some cases, the electrode process is irreversible (see entries 1–3, 9, 10), whereas it is reversible in others (entries 4–8). The ligands L and *L* are not electroactive at the potentials employed for the metal carbonyls in Table 2. Let us now examine the

TABLE 2

CYCLIC VOLTAMMETRIC PARAMETERS FOR THE VARIOUS METAL CARBONYLS [a]

	$LM(CO)_n$	Solvent	E_p^{ox} (V)	$\frac{1}{2}(E_p^{ox} + E_p^{red})$ (V)	i_p^a/i_p^c
1.	*cis*-$(CO)_4Mo(py)_2$	MeCN	0.57 [b]	irreversible	> 10 [c]
2.	*cis*-$(CO)_4Mo(CNCMe_3)_2$	MeCN	0.96 [b]	irreversible	> 10 [c]
3.	$(\eta^5\text{-}C_5H_4Me)Mn(CO)_2(THF)$	THF	0.03	irreversible	> 10 [d]
4.	$(\eta^5\text{-}C_5H_4Me)Mn(CO)_2(py)$	THF	0.17	0.11	1.0 [e]
5.	$(\eta^5\text{-}C_5H_4Me)Mn(CO)_2(MeCN)$	MeCN	0.22	0.19	1.0 [c,d]
6.	$(\eta^5\text{-}C_5H_4Me)Mn(CO)_2[P(OMe)Ph_2]$	MeCN	0.65	0.62	1.0 [d]
7.	$(\eta^5\text{-}C_5H_4Me)Mn(CO)_2(py)$	Me_2CO	0.14	0.11	1.0 [c,d]
8.	$(\eta^5\text{-}C_5H_4Me)Mn(CO)_2(CNCMe_3)$	Me_2CO	0.59	0.54	1.0 [d]
9.	$(\eta^5\text{-}C_5H_5)Re(CO)_2(py)$	Me_2CO	0.44	irreversible	> 10 [e]
10	$(\eta^5\text{-}C_5H_5)Re(CO)_2(PPh_3)$	Me_2CO	0.86	irreversible	> 10 [e]

[a] Cyclic voltammetry was performed at a Pt bead with solutions 10^{-3} *M* in metal carbonyl and 0.1 *M* in supporting electrolyte (tetraethylammonium perchlorate for MeCN or acetone, tetrabutylammonium perchlorate for THF). The scan rate was 100 mV s^{-1} at 22°C. Potentials are reported relative to the Cp_2Fe/Cp_2Fe^+ couple taken to have $\frac{1}{2}(E_p^{ox} + E_p^{red})$ 0.31 V versus saturated NaCl SCE in all solvents. [b] Scan rate of 200 mV s^{-1}. [c] Ref. 7. [d] Ref. 8. [e] This work.

cyclic voltammetric behavior of the electrocatalytic systems presented in Table 1, first with the metal carbonyl $LM(CO)_4$ alone, and then in the presence of added *L*.

Figure 1 illustrates the effect of added t-butyl isocyanide on the cyclic voltammogram of *cis*-$(py)_2Mo(CO)_4$. Two phenomena are observed. First, the peak current for the irreversible wave R of *cis*-$(py)_2Mo(CO)_4$ with E_p 0.57 V is reduced from 70 μA in (a) to only 15 μA in (b); and second, a new irreversible wave I occurs at E_p 0.76 V. However, The latter does not correspond to the CV wave for the disubstitution product P *cis*-$(t\text{-BuNC})_2Mo(CO)_4$ which is proven product of the bulk experiment, previously described in Table 1, entry 1. Its irreversible cyclic voltammogram occurs at E_p 0.96 V as shown in Fig. 1 (c). We propose that the anodic wave with E_p 0.76 V corresponds to the buildup of the mono-substitution product (t-BuNC)(py)$Mo(CO)_4$ on the timescale of the CV experiment.

$$\begin{matrix} py \\ py \end{matrix}\!\!\rangle Mo(CO)_4 + \text{t-BuNC} \xrightarrow{[E]} \text{t-BuNC}\!\!\langle \begin{matrix} \\ py \end{matrix} Mo(CO)_4 + \text{py, etc.} \qquad (9)$$

Indeed similar sequential substitution has been clearly demonstrated to occur in related systems (e.g., *fac*-$(MeCN)_3W(CO)_3$ with t-BuNC and *cis*-$(MeCN)_2W(CO)_4$ with PPh_3 [7].)

Figure 2 shows that the effect of added pyridine on the cyclic voltammogram of (η^5-C_5H_4Me)$Mn(CO)_2$(THF), in which the irreversible wave R at E_p 0.03 V of the

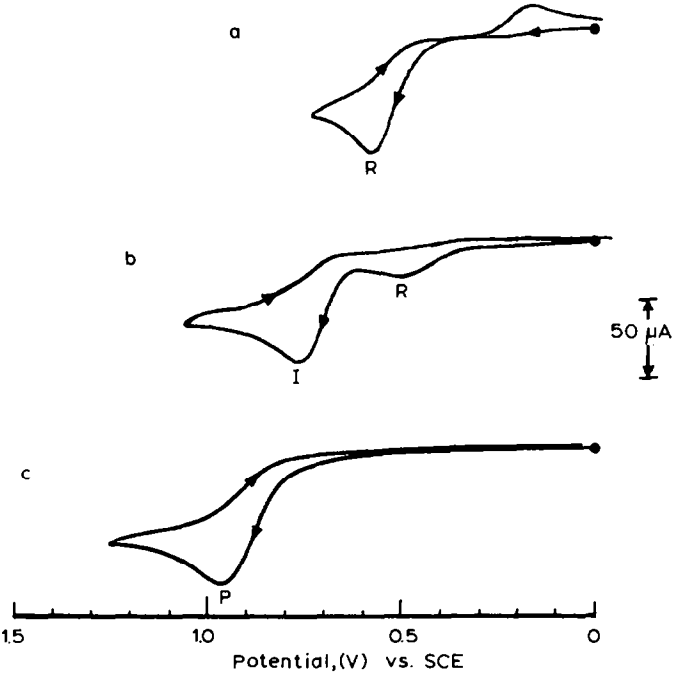

Fig. 1. (a) Initial scan cyclic voltammogram of 2×10^{-3} *M* *cis*-$(py)_2Mo(CO)_4$ in acetonitrile containing 0.1 *M* tetraethylammonium perchlorate (TEAP) at 20°C and a scan rate of 200 mV s^{-1}; (b) Same as in a, but with a 10-fold excess of t-BuNC added; (c) Cyclic voltammogram of authentic $(t\text{-BuNC})_2Mo(CO)_4$. The anodic wave of the reactant is indicated as R, and that of the ultimate product as P. For the anodic peak labelled I, see text.

reactant in (a) is almost completely supplanted by the reversible CV wave P of the product (η^5-C_5H_4Me)$Mn(CO)_2$(py) with E^0 0.11 V.

In Fig. 3, the reversible oxidation of (η^5-C_5H_4Me)$Mn(CO)_2$(NCMe) at E^0 0.19 V is rendered totally irreversible by the addition of the phosphine nucleophile $P(OMe)Ph_2$. The anodic peak current for the reactant is reduced drastically by the presence of only a slight molar excess of $P(OMe)Ph_2$ in b, similar to the observations in Figs. 1 and 2. The CV wave in Fig. 3(b) at $(E_p^{ox} + E_p^{red})/2 = 0.62$ V corresponds to reversible oxidation of (η^5-C_5H_4Me)$Mn(CO)_2[P(OMe)Ph_2]$, which is the proven product obtained in the bulk electrolysis experiment described in entry 3, Table 1. Figure 3(c) shows the effect of a large (~ 5-fold) excess of $P(OMe)Ph_2$. The anodic process corresponding to the reactant is now scarcely visible, and the CV wave corresponding to the product has acquired an elongated less reversible appearance.

Fig. 2

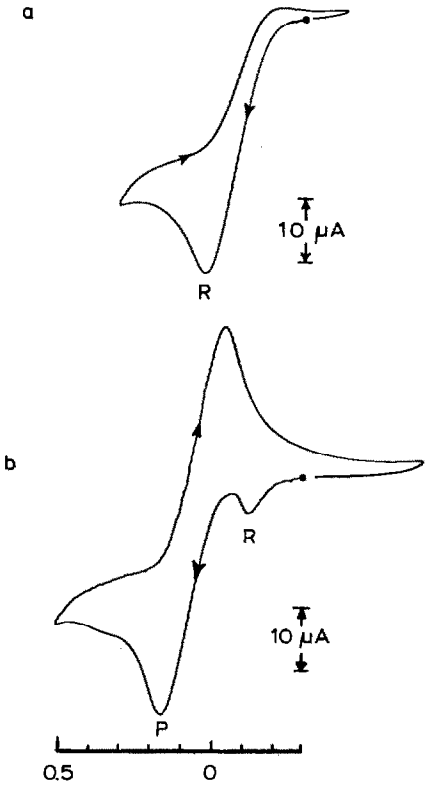

Fig. 3

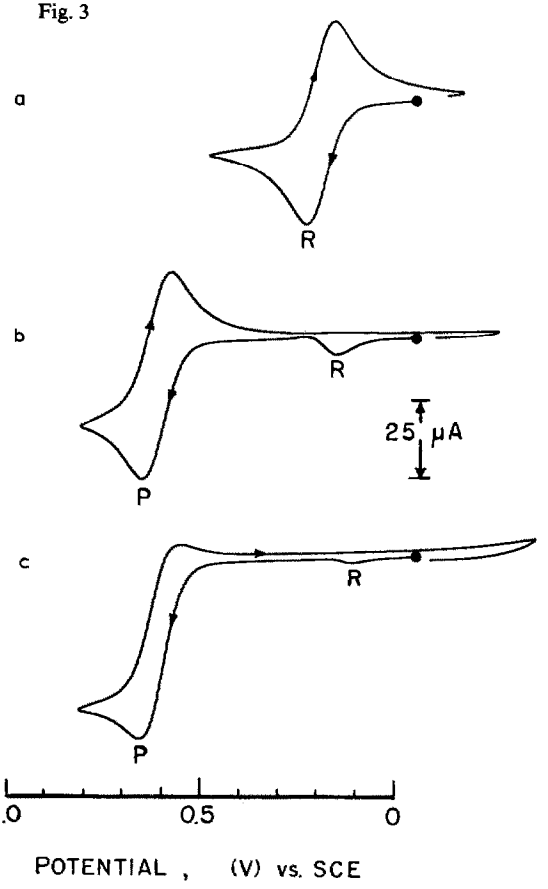

Fig. 2. (a) Initial scan cyclic voltammogram of ~ 1×10^{-3} *M* (η^5-C_5H_4Me)$Mn(CO)_2$(THF) in tetrahydrofuran containing 0.1 *M* tetra-n-butylammonium perchlorate at 20°C and a scan rate of 100 mV s^{-1}; (b) Same as above but with added pyridine (1.6×10^{-2} *M*). The anodic wave of the reactant is labelled R and that of the product (η^5-C_5H_4Me)$Mn(CO)_2$(py) as P.

Fig. 3. (a) Reversible cyclic voltammogram of 1.26×10^{-3} *M* (η^5-C_5H_4Me)$Mn(CO)_2$(NCMe) in acetonitrile containing 0.1 *M* TEAP at 21°C and a scan rate of 100 mV s^{-1}; (b) Same as in a, but with added $P(OMe)Ph_2$ (2.02×10^{-3} *M*); (c) Same as in a, but with excess $P(OMe)Ph_2$ (7.07×10^{-3} *M*).

We will show in the next section how such an elongation of the CV wave arises from the homogeneous oxidation of the excess phosphine by the cationic intermediate $(\eta^5\text{-}C_5H_4Me)Mn(CO)_2[P(OMe)Ph_2]^+$.

The effect of added t-butyl isocyanide on the cyclic voltammogram of $(\eta^5\text{-}C_5H_4Me)Mn(CO)_2(py)$ is shown in Fig. 4. This electrocatalytic system in eq. 10 might be expected to behave similarly to that illustrated in Figs., 3(a) and 3(b), since

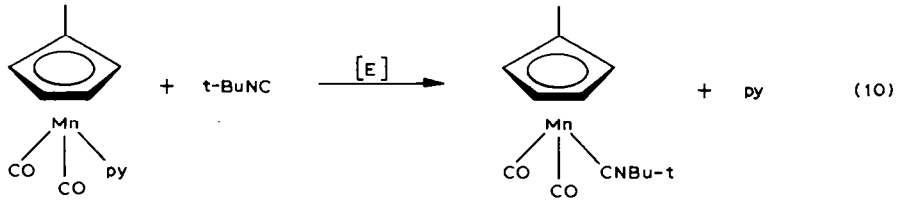

(10)

the electrode process is observed (see Table 2) to be reversible for both the reactant with E^0 0.11 V as well as the product $(\eta^5\text{-}C_5H_4Me)Mn(CO)_2(CNBu\text{-}t)$ with E^0 0.54 V. Instead, the product wave is completely irreversible in Fig. 4(b). We shall show that this peculiar behavior is completely accountable by the action of free t-BuNC upon the radical-cation intermediate, i.e., $(\eta^5\text{-}C_5H_4Me)Mn(CO)_2(CNBu\text{-}t)^+$ (vide infra).

The preceding four examples represent typical illustrations of cyclic voltammetric behavior which can be associated with electrocatalytic ligand substitution in metal carbonyls. Although the shapes of the cyclic voltammograms may appear somewhat disparate, they indeed share one important characteristic in common. Independent of whether the initial electron transfer is irreversible (Figs. 1 and 2) or reversible (Figs. 3 and 4), the anodic peak current associated with the reactant $LM(CO)_n$ is drastically reduced in magnitude by added uncleophile L when the $\bar{E}C\bar{E}$ substitution process described by Scheme 1 is rapid on the CV timescale.

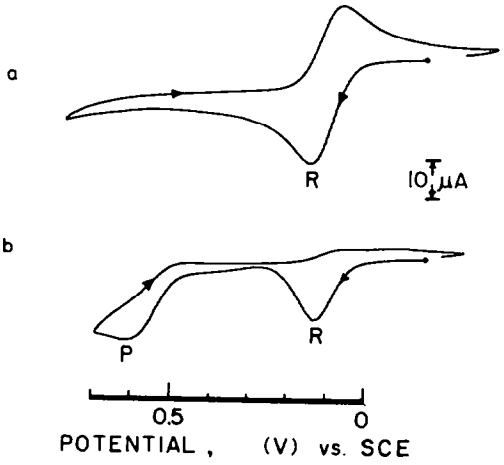

Fig. 4. (a) Initial scan cyclic voltammogram of 1.34×10^{-3} M $(\eta^5\text{-}C_5H_4Me)Mn(CO)_2(py)$ in acetone containing 0.1 M TEAP at 20°C and a scan rate of 100 mV s^{-1}; (b) Same as in a, except with added t-BuNC (3.84×10^{-3} M).

Since the current is directly related to the concentration of the reactant $LM(CO)_n$, unique insight into the mechanism of electrocatalysis is provided by cyclic voltammetry. Thus the cyclic voltammetry in the presence of added ***L*** demonstrates three important conclusions embodied in Scheme 1. First, the cathodic wave in Figs. 3(a) and 4(a) corresponding to the reduction of the radical-cation $LM(CO)_n^+$ disappears entirely in the presence of added ***L***, as shown by the absence of this component in Figs. 3(b) and 4(b). In other words, the radical cation is observed to have an exceedingly short lifetime in the presence of added nucleophile. Second, the wave corresponding to the oxidation of the reactant $LM(CO)_n$ gradually decreases in size as the concentration of ***L*** is increased, which indicates that $LM(CO)_n$ is being depleted by some alternative process which does not require the net passage of current. It is important to emphasize that this highly efficient process (compare the first wave in Figs. 3(a), 3(b) and 3(c)) is operative in the vicinity of the electrode since these metal carbonyls in the presence of ***L*** are otherwise very stable in the bulk solution (vide supra). Third, the substitution product $\boldsymbol{L}M(CO)_n$ is also being generated in high yields in the region adjacent to the electrode, as witnessed by the appearance of the wave corresponding to the oxidation of $\boldsymbol{L}M(CO)_n$. Significantly, the direction of current flow demonstrates the product is ultimately produced in the reduced form. One is thus forced to the conclusion that electrocatalysis stems from the lability of the radical cation of the reactant $LM(CO)_n^+$ (as delineated in eq. 3 of Scheme 1), and that the generation of the neutral product $\boldsymbol{L}M(CO)_n$ derives from either a homogeneous or heterogeneous electron transfer process (as described by eqs. 4 and 5, respectively.) Thus valuable mechanistic information, albeit qualitative, is readily obtained from the cyclic voltammetry of metal carbonyl solutions in the presence of added nucleophiles, independent of whether the electrochemical characteristics of the system follow reversible behavior or not. Indeed we have found cyclic voltammetry to be an excellent diagnostic tool in our search for ligand exchange processes induced by electron transfer.

Having described the electrocatalytic phenomenon by bulk and transient electrochemical methods, we turn to the quantitative description of the kinetics associated with the ligand substitution of metal carbonyls. Let us now consider how digital simulation of the cyclic voltammograms can be used to provide a more quantitative understanding of the kinetics of electrocatalysis.

Electrocatalytic kinetics of ligand substitution by the digital simulation of cyclic voltammograms

We proceed from the established mechanism presented in Scheme 1 for the $\vec{E}C\vec{E}$ process under study. The complex kinetics of the electrocatalytic substitution of metal carbonyls can be digitally simulated by the method of finite differences, as described by Feldberg [14,15]. For convenience in the presentation, the reactant and the substitution product have been abbreviated as LM and $\boldsymbol{L}M$, respectively, and the appropriate rate constants for each step labelled in the following manner:

SCHEME 1′

$$LM \overset{k_s(1)}{\rightleftharpoons} LM^+ \tag{11}$$

$$LM^+ + \boldsymbol{L} \underset{k_{-1}}{\overset{k_1}{\rightleftharpoons}} \boldsymbol{L}M^+ + L \tag{12}$$

$$\boldsymbol{L}M^+ + LM \underset{k_{-2}}{\overset{k_2}{\rightleftharpoons}} \boldsymbol{L}M + LM^+ \tag{13}$$

$$\boldsymbol{L}M^+ \overset{k_s(2)}{\rightleftharpoons} \boldsymbol{L}M \tag{14}$$

The parameters required for the construction of the theoretical cyclic voltammograms according to this scheme are [16–23]: $C_{i,j}$ the initial concentrations of LM and $\boldsymbol{L}$ respectively, v the scan rate, $E^0_{m,n}$ the formal potentials for the redox couples LM/LM^+ and $\boldsymbol{L}M/\boldsymbol{L}M^+$, β the respective transfer coefficients. D the diffusion coefficient for each of the six species, $k_s(1)$ and $k_s(2)$ the standard rate constants for heterogeneous electron transfer of the redox couples, and the homogeneous rate constants k_1 and k_{-1} for ligand exchange and k_2 and k_{-2} for electron transfer. Indeed we have found that the electrocatalytic kinetics for ligand substitution can be computer simulated when the metal carbonyls possess the following characteristics: Both LM and $\boldsymbol{L}M$ exhibit reversible CV waves, and thus E^0 can be reliably and readily estimated from $(E_p^{ox} + E_p^{red})/2$ and values of k_s can be determined from the sweep dependence of $E_p^{ox} - E_p^{red}$ by standard electrochemical procedures [24,25]. Electron transfer between LM and $\boldsymbol{L}M^+$ in eq. 13 is essentially unidirectional and k_{-2} is unimportant, because the difference in the electrode potentials for the couples LM/LM^+ and $\boldsymbol{L}M/\boldsymbol{L}M^+$ is large (see Table 2). Likewise, the ligand exchange process in eq. 12 is unidirectional, and the contribution from k_{-1} is negligible. (Small values of k_{-1} and k_{-2} are consistent with the observation that the equilibrium constant K_{eq} for the overall ligand exchange process in eq. 1 is immeasurably large for the systems listed in Table 1.) Chain termination process can be ignored, since the substitution reactions have quasi-infinite kinetic chain lengths, as reflected by the high current efficiencies in the coulometric experiments listed in Table 1. Other studies have shown that the digital simulation is not critically dependent on the variations in the parameters β and D [26]. As a result, only two quantities, the rate constants k_1 and k_2, are needed for the construction of theoretical cyclic voltammograms for the electrocatalysis of ligand substitution.

Ligand substitution of acetonitrile by methoxydiphenylphosphine. The effectiveness of the digital simulation procedure is illustrated in Fig. 5, in which the experimental (left side) and theoretical (right side) cyclic voltammograms are compared for a solution of 1.26×10^{-3} M $(\eta^5\text{-}C_5H_4Me)Mn(CO)_2(NCMe)$ in acetonitrile undergoing electrocatalytic substitution by 2.02×10^{-3} M $P(OMe)Ph_2$ at two different scan rates of (a) 200 mV s^{-1} and (b) 800 mV s^{-1}. When the concentration of the added nucleophile is increased by ~ 3-fold to 7.07×10^{-3} M, a higher scan rate of 1000 mV s^{-1} is required to maintain a similar CV behavior, as shown in Fig. 5(c). It is important to note that the upper three theoretical cyclic voltammograms shown on the right side of Fig. 5 could be successfully computer simulated using common values of the homogeneous rate constants k_1 2.5×10^4 M^{-1} s^{-1} and k_2 2×10^5 M^{-1} s^{-1} for ligand exchange and electron transfer processes in eqs. 12′ and 13′, respectively.

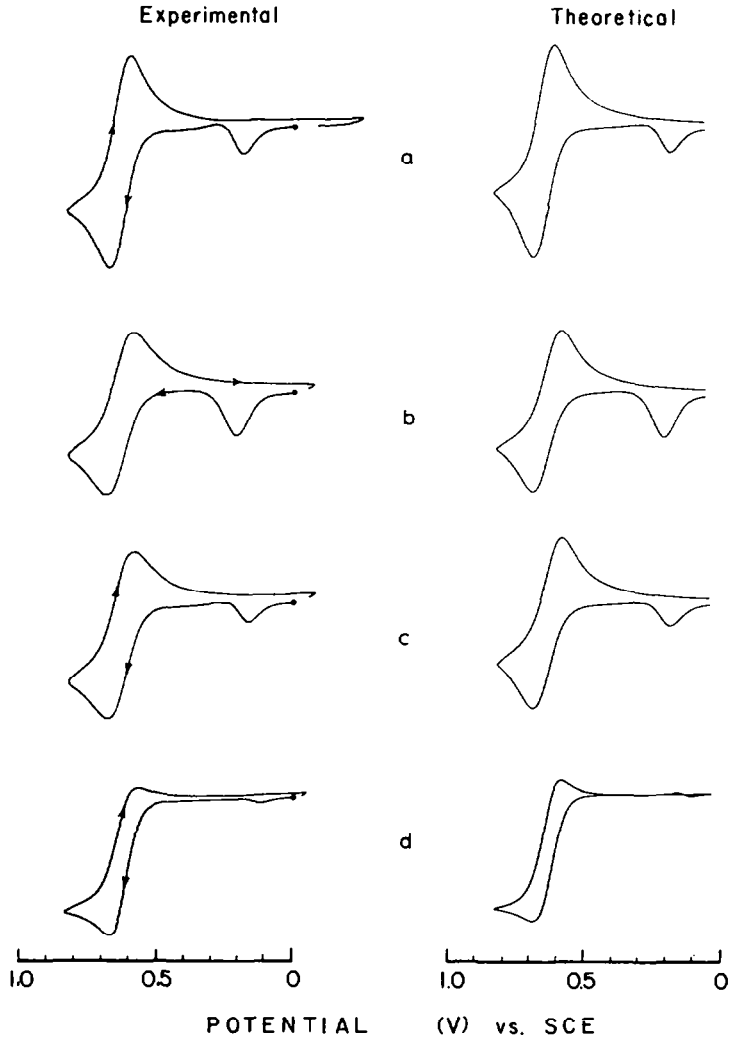

Fig. 5. Experimental and theoretical cyclic voltammograms of solutions containing 1.26×10^{-3} *M* (η^5-C_5H_4Me)$Mn(CO)_2$(NCMe) in acetonitrile containing 0.1 *M* TEAP at 25°C and various amounts of added $P(OMe)Ph_2$ and at varying scan rates: (a) 2.02×10^{-3} *M* $P(OMe)Ph_2$ and 200 mV s^{-1}; (b) 2.02×10^{-3} *M* $P(OMe)Ph_2$ and 800 mV s^{-1}; (c) 7.07×10^{-3} *M* $P(OMe)Ph_2$ and 1000 mV s^{-1}; (d) 7.07×10^{-3} *M* $P(OMe)Ph_2$ and 100 mV s^{-1}.

$$\overline{Mn}(NCMe)^+ + P(OMe)Ph_2 \xrightarrow{k_1} \overline{Mn}[P(OMe)Ph_2]^+ + MeCN \qquad (12')$$

$$\overline{Mn}[P(OMe)Ph_2]^+ + \overline{Mn}(NCMe) \xrightarrow{k_2} \overline{Mn}[P(OMe)Ph_2] + \overline{Mn}(NCMe)^+ \qquad (13')$$

$$\left(\overline{Mn} = (\eta^5\text{-}C_5H_4Me)Mn(CO)_2\right)$$

Since k_2 is at least an order of magnitude larger than k_1, the ligand exchange process in eq. 12′ clearly represents the rate-limiting step in electrocatalysis. Indeed,

rather large changes in k_2 effect only minor changes in the computed cyclic voltammograms, provided the values of k_2 were always $> 10k_1$.

Upon lowering the CV scan rate of the same solution used in Fig. 5(c), the anodic peak current of the first wave R diminished as expected, but the second wave P experienced an apparent elongation shown on the left side of Fig. 5(d). Such a distortion of the CV wave in an otherwise well-behaved electrochemical system arises from intrusion of an added kinetic complication. Indeed the elongated shape of the CV wave such as that in Fig. 5(d) has been previously described by Nicholson and Shain [27] for the general case, in which the electrode process consisted of a reversible electron transfer followed by the chemical regeneration of the reduced species (Case VI in their paper [27]). For the system in question, the intruding process is the homogeneous oxidation of the added phosphine by the radical cation of the product formed in eq. 12′, viz.,

$$\overline{\mathrm{Mn}}[\mathrm{P(OMe)Ph_2}]^+ + \mathrm{P(OMe)Ph_2} \xrightarrow{k_3} \overline{\mathrm{Mn}}[\mathrm{P(OMe)Ph_2}] + \mathrm{P(OMe)Ph_2}^+, \text{ etc.} \quad (15)$$

Inclusion of this step with a rate constant k_3 1.05×10^2 M^{-1} s^{-1}, in addition to those in Scheme 1, led to the successful simulation of the cyclic voltammogram shown on the right side of Fig. 5(d) (see Experimental section). Note that the electrochemical and kinetic parameters used for the computer simulation in Fig. 5(d) are the same as those employed in Figs. 5(a)–5(c).

The kinetic effect of the competing process in eq. 15 is unusual since it leads to the oxidative consumption of the phosphine at electrode potentials which are substantially less (i.e., more negative) than otherwise required in the absence of metal carbonyl.

Such an interesting electrochemical phenomenon leading to the "catalytic wave" in Fig. 5(d) has been referred to as "redox catalysis" * [28,29]. (It must be emphasized that the cyclic voltammogram in Fig. 5(d) cannot be simulated without taking explicitly into account such a competition from the oxidation of the added phosphine.)

Redox catalysis of phosphine oxidation by a metal carbonyl. In order to further delineate this interesting electrochemical phenomenon associated with the ligand substitution of metal carbonyls, we examined next the CV behavior of a simpler system involving only a phosphine metal complex in the presence of its own added phosphine. For the manganese complex $(\eta^5\text{-}C_5H_4Me)Mn(CO)_2[PMePh_2]$, the process leading to redox catalysis would then derive from the electron transfer in eq. 16

$$\overline{\mathrm{Mn}}[\mathrm{PMePh_2}]^+ + \mathrm{PMePh_2} \rightarrow \overline{\mathrm{Mn}}[\mathrm{PMePh_2}] + \mathrm{PMePh_2}^+ \quad (16)$$

As shown by the sequence of cyclic voltammograms in Fig. 6, the effect of increasing concentrations of PMe_2Ph_2 is to suppress the cathodic component of the reversible wave associated with $(\eta^5\text{-}C_5H_4Me)Mn(CO)_2[PMePh_2]$ in (a). Concomitantly, the anodic peak current increases substantially (note the change of the current scale in (c)), as a result of the electroactive, neutral $(\eta^5\text{-}C_4H_5Me)$-$Mn(CO)_2[PMePh_2]$ being constantly regenerated at the electrode according to eq. 16.

* Catalysis in this electrochemical context refers to the acceleration of a rate process, as reflected in the application of a lower electrode potential, i.e. driving force.

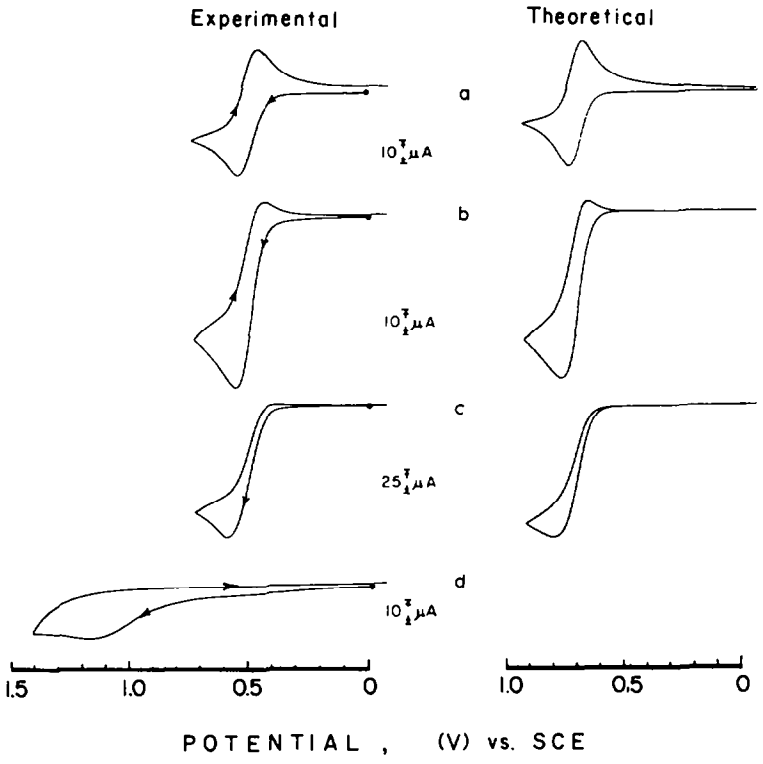

Fig. 6. Quantitative kinetic treatment of redox catalysis for phosphine oxidation by a metal carbonyl, showing the experimental (left side) and theoretical (right side) of cyclic voltammograms derived from (a) 1.49×10^{-3} *M* (η^5-C_5H_4Me)$Mn(CO)_2$[$PMePh_2$] in acetone containing 0.1 *M* TEAP at 20°C with (b) 2.16×10^{-3} *M* and (c) 7.55×10^{-3} *M* of added $PMePh_2$ at a scan rate of 100 mV s^{-1}; (d) Cyclic voltammogram of $PMePh_2$ alone (2.16×10^{-3} *M*) in acetone containing 0.1 *M* TEAP at 100 mV s^{-1} and 20°C. See text for the significance of E_p for $PMePh_2$.

The mechanism for the redox catalysis of phosphine oxidation is summarized by Scheme 2, and the digital simulations of the cyclic voltammograms based on

SCHEME 2

$$ML \overset{k_s}{\rightarrow} ML^+ \tag{17}$$

$$ML^+ + L \overset{k_3}{\rightarrow} ML + L^+, \text{ etc.} \tag{18}$$

Feldberg's technique are shown on the right side of Fig. 6a–6c using only a single value for the electron transfer rate constant $k_3 = 10^3\ M^{-1}\ s^{-1}$.

The validity of this kinetic analysis was substantiated by an independent galvanostatic experiment shown in Fig. 7, in which the bulk oxidation of $PMePh_2$ was carried out at the electrode potential of ~ 0.4 V which corresponds to the foot of the reversible CV wave for (η^5-C_5H_4Me)$Mn(CO)_2$[$PMePh_2$]. Since the electrochemical oxidation of $PMePh_2$ was negligible at these potentials (See the cyclic voltammogram of $PMePh_2$ in Fig. 6(d)), the current must have arisen solely from the oxidation

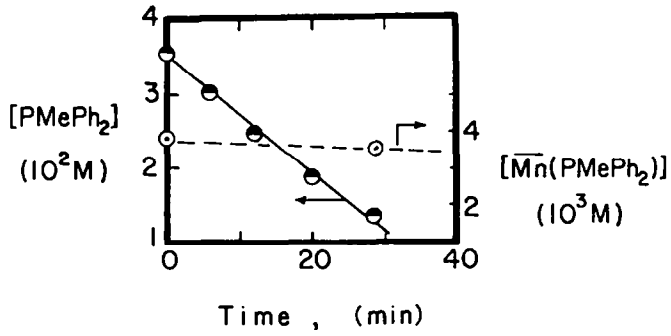

Fig. 7. Concentration changes during the controlled-current electrolysis of a solution containing 5.6×10^{-5} mol of $(\eta^5\text{-}C_5H_4Me)Mn(CO)_2[PMePh_2]$ (⊙) and 5.3×10^{-4} mol of $PMePh_2$ (●) in 15 ml of acetone with 0.1 *M* TEAP at 10 mA and 22°C. The potential of the platinum working electrode was initially at 0.38 V and rose to 0.41 V after 29 min.

of the manganese complex. Nevertheless, the results in Fig. 7 show that only the phosphine, not the manganese carbonyl, is consumed. It is important to reemphasize that the oxidation of $PMePh_2$ by such a redox catalysis occurs at an electrode potential of ~ 0.4 V which is significantly less positive than that (~ 1 V) required for the phosphine alone. (Compare the E_p of the anodic waves in Figs. 6(c) and 6(d)!).

Redox catalysis during the ligand substitution of pyridine by methyldiphenylphosphine. The evaluation of the electron transfer rate constant k_3 in eq. 16 for phosphine oxidation, as described in the preceding section, allows us to simulate now the entire CV wave for electrocatalysis of ligand substitution of $(\eta^5\text{-}C_5H_4Me)Mn(CO)_2[py]$ by the phosphine $PMePh_2$, including the "catalytic wave effect" induced by the latter. Figure 8 shows the well-behaved, reversible cyclic voltammograms of both the reactant R ($(\eta^5\text{-}C_5H_4Me)Mn(CO)_2[py]$) as well as the product P $(\eta^5\text{-}C_5H_4Me)Mn(CO)_2[PMePh_2]$ in (a) and (d), respectively. The cyclic voltammograms of $(\eta^5\text{-}C_5H_4Me)Mn(CO)_2[py]$ in the presence of various amounts of added $PMePh_2$ are shown in (b) and (c). Qualitatively, the striking appearance of the CV waves in Figs. 8(b) and 8(c) is akin (albeit highly exaggerated) to that previously described for ligand substitution of $(\eta^5\text{-}C_5H_4Me)Mn(CO)_2(NCMe)$ by the related phosphine $P(OMe)Ph_2$ in Fig. 5(d). Accordingly, the digital simulation of the cyclic voltammograms was carried out with the appropriate kinetic scheme described below.

SCHEME 3

$$\overline{Mn}(py) \xrightarrow{k_s(1)} \overline{Mn}(py)^+ \tag{19}$$

$$\overline{Mn}(py)^+ + PMePh_2 \xrightarrow{k_1} \overline{Mn}(PMePh_2)^+ + py \tag{20}$$

$$\overline{Mn}(PMePh_2)^+ + Mn(py) \xrightarrow{k_2} \overline{Mn}(PMePh_2) + \overline{Mn}(py)^+, \text{ etc.} \tag{21}$$

$$\overline{Mn}(PMePh_2)^+ + PMePh_2 \xrightarrow{k_3} \overline{Mn}(PMePh_2) + PMePh_2^+, \text{ etc.} \tag{16}$$

$$\overline{Mn}(PMePh_2) \xrightarrow{k_s(2)} \overline{Mn}(PMePh_2)^+ \tag{22}$$

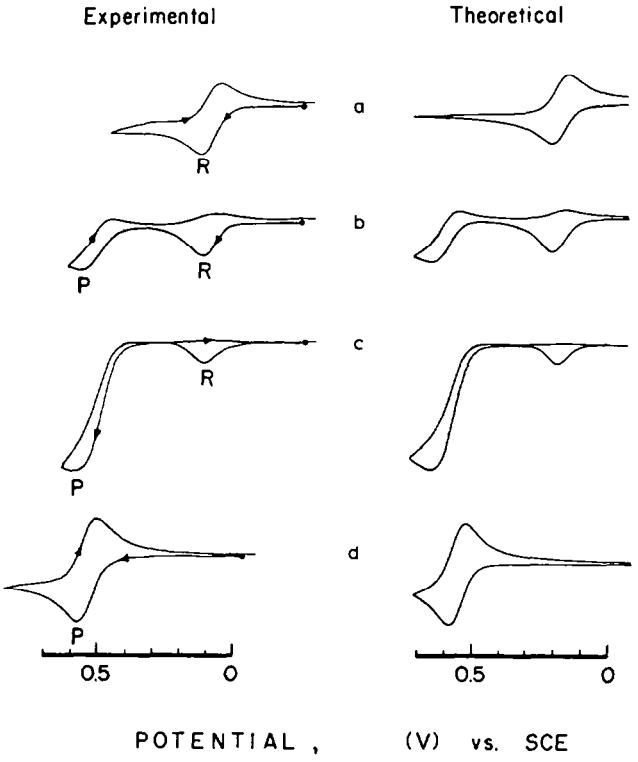

Fig. 8. Redox catalysis during the ligand substitution of 1.1×10^{-3} *M* (η^5-C_5H_4Me)$Mn(CO)_2$[py] in the presence of various amounts of added $PMePh_2$ in acetonitrile containing 0.1 *M* TEAP at 20°C. (a) none; (b) 1.24×10^{-3} *M*; (c) 5.2×10^{-3} *M*. Left figures are experimental cyclic voltammograms recorded at 50 mV s^{-1}, and those only on the right side are computer simulated with k_1 4×10^2 M^{-1} s^{-1}, k_2 2×10^5 M^{-1} s^{-1}, and k_3 1×10^3 M^{-1} s^{-1}. The reversible cyclic voltammogram of the product (η^5-C_5H_4Me)$Mn(CO)_2$[$PMePh_2$] under the same conditions is shown in d.

The excellent fit of the theoretical cyclic voltammograms shown on the right side of Fig. 8 to the experimental ones (left side) derive with the use of only one set of kinetic parameters (see Experimental section). It is singularly noteworthy that the optimized value of the electron transfer rate constant k_3 1×10^3 M s^{-1} for eq. 16 is essentially the same as that ($1.5 \pm 0.5 \times 10^3$ M^{-1} s^{-1}) obtained in the foregoing section by an independent evaluation.

Electrocatalytic substitution of a metal carbonyl by t-butyl isocyanide. The effect of t-butyl isocyanide on the ligand substitution of $\overline{Mn}$(py) was presented in Fig. 4(b). In order to simulate this cyclic voltammogram, we first established the CV behavior of the ligand-substitution product, that is (η^5-C_5H_4Me)$Mn(CO)_2$[CNBu-t], in the presence of added t-butyl isocyanide. Figure 9(a) shows the well-behaved, reversible cyclic voltammogram of (η^5-C_5H_4Me)$Mn(CO)_2$[CNBu-t] with E^0 0.54 V. In. the presence of added t-butyl isocyanide, the cathodic component of the CV wave P in Fig. 9(b) was obliterated in a manner reminiscent of redox catalyses described in the foregoing sections above. However the near constancy of the anodic current of P, as

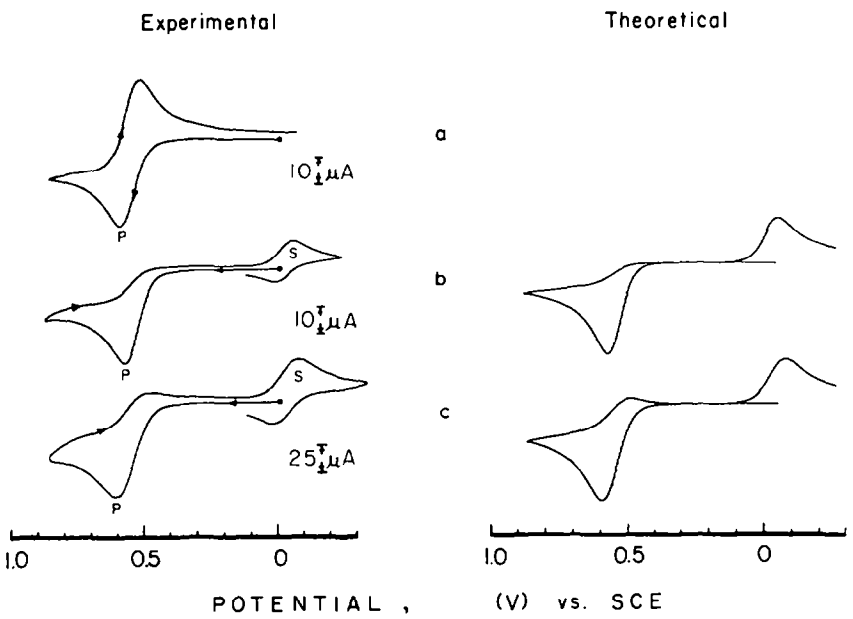

Fig. 9. Experimental and theoretical single scan cyclic voltammograms of 1.28×10^{-3} M (η^5-C_5H_4Me)Mn(CO)$_2$[CNBu-t] in acetone containing 0.1 M TEAP at 20°C: (a) without added t-BuNC and a scan rate of 100 mV s^{-1}; (b) with 3.84×10^{-3} M added to t-BuNC and 100 mV s^{-1}; (c) as in b but at a scan rate of 800 mV s^{-1}. Note the current scale is changed and the return wave S of the product is not included in the theoretical cyclic voltammograms.

well as the growth of a new wave S at E^0 −0.03 V shown in Fig. 9(b), do not support a redox catalytic process. Instead this CV behavior is diagnostic of a kinetic phenomenon in which the product radical cation $\overline{Mn}$[CNBu-t]$^+$ is itself consumed in a bimolecular reaction with free t-butyl isocyanide to afford a non-electroactive product. Indeed the computer simulations of the cyclic voltammograms shown on the right side of Fig. 9 were carried out by invoking such a side reaction with a rate constant k_4 2×10^3 M^{-1} s^{-1}. Although the success of the digital simulation does not depend on the proof of product identity, independent experiments described in the Experimental section suggest that it derived from disubstitution, viz.,

$$(\eta^5\text{-}C_5H_4Me)Mn(CO)_2[CNBu\text{-}t]^+ + \text{t-BuNC} \xrightarrow{k_4}$$

$$(\eta^5\text{-}C_5H_4Me)Mn(CO)[CNBu\text{-}t]_2{}^+ + CO \qquad (23)$$

Indeed the successful simulations of the cyclic voltammograms in Fig. 9 allows the complex kinetics associated with the substitution of the pyridine complex (η^5-C_5H_4Me)Mn(CO)$_2$(py) by t-butyl isocyanide to be treated quantitatively as shown in scheme 4.

The experimental and theoretical cyclic voltammograms for this system are compared on the left and right sides, respectively, of Fig. 10 at two scan rates. (Note the presence of the CV wave S as only a minor component in Fig. 10(a)). The digital simulations employed the same rate constant of $k_4 = 2 \times 10^3$ M^{-1} s^{-1}, independently evaluated for eq. 23 in Fig. 9, and an optimized ligand exchange rate constant of k_1 5.0×10^2 M^{-1} s^{-1}. The agreement is somewhat modest, probably owing to the

SCHEME 4

$$\overline{\text{Mn}}(\text{py}) \xrightarrow{k_s(1)} \overline{\text{Mn}}(\text{py})^+ \tag{24}$$

$$\overline{\text{Mn}}(\text{py})^+ + \text{t-BuNC} \xrightarrow{k_1} \overline{\text{Mn}}(\text{CNBu-t})^+ + \text{py} \tag{25}$$

$$\overline{\text{Mn}}(\text{CNBu-t})^+ + \overline{\text{Mn}}(\text{py}) \xrightarrow{k_2} \overline{\text{Mn}}(\text{CNBu-t}) + \overline{\text{Mn}}(\text{py})^+, \text{ etc.} \tag{26}$$

$$\overline{\text{Mn}}(\text{CNBu-t})^+ + \text{t-BuNC} \xrightarrow{k_4} (\eta^5\text{-}C_5H_4\text{Me})\text{Mn}(\text{CO})(\text{CNBu-t})_2{}^+ + \text{CO} \tag{23}$$

$$\overline{\text{Mn}}(\text{CNBu-t}) \xrightarrow{k_2(2)} \overline{\text{Mn}}(\text{CNBu-t})^+ \tag{27}$$

electrode characteristics which generally degraded during the course of the CV experiment. Although the CV characteristics of the acetonitrile complex (η^5-C_5H_4Me)Mn(CO)$_2$(NCMe) with added t-butyl isocyanide were better in acetonitrile, the ligand exchange rate ($k_1 > 10^5$ M^{-1} s^{-1}) was unfortunately too fast to be adequately evaluated by the numerical method employed in this study. Although further substitution of the product by t-butyl isocyanide (such as the reaction in eq. 23), can be observed in the CV experiments, the process is fortunately too slow to interfere significantly with the chain substitution carried out in the bulk, as indicated by the current efficiency in excess of 60 in Table 1, entry 4. Furthermore the rates of electron transfer from the neutral reactant ML to the product radical cation ML^+ (i.e., k_2) is sufficiently rapid to obviate such side reactions except at very low concentrations of ML. Nonetheless, CV studies with other metal carbonyl derivatives, including those with carbon monoxide, trialkylphosphine and trialkyl phosphite ligands, indicate that substitutions by alkyl isocyanides are facile and a general phenomenon. As a typical example, the reversible cyclic voltammogram of (η^5-C_5H_4Me)Mn(CO)$_3$ at E^0 1.15 V in acetonitrile containing 0.1 M TEAP, is rendered

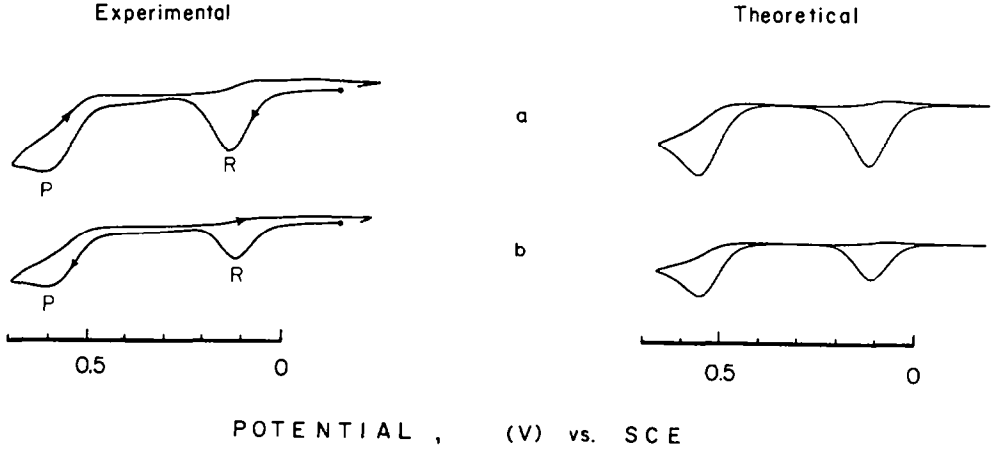

Fig. 10. Experimental (left side) and theoretical (right side) cyclic voltammograms for electrocatalysis in the ligand substitution of 1.34×10^{-3} M (η^5-C_5H_4Me)Mn(CO)$_2$(py) by 3.84×10^{-3} M of added t-butyl isocyanide in acetone containing 0.1 M TEAP at 20°C and scan rates of (a) 100 mV s^{-1} and (b) 50 mV s^{-1}.

completely irreversible by the addition of t-butyl isocyanide at −28°C. On the reverse CV scan, a reversible redox couple at −0.03 V is observed, which is identical to that observed for the CV wave S in Figs. 9(b) and 9(c).

Discussion

Ligand substitution of a metal carbonyl and its derivatives in the most general form represents an exchange process, in which the notation ML designates the metal

$$ML + \boldsymbol{L} \rightleftharpoons M\boldsymbol{L} + L \tag{28}$$

carbonyl, and L represents the displaced ligand and $\boldsymbol{L}$ the added nucleophile. Electrocatalysis of ligand substitution thus refers to the promotion of eq. 28 at an electrode with minimal consumption of current, under conditions in which the conventional thermal processes [1–3] are either nonexistent or unimportant.

Bulk electrolysis at either constant current or voltage allows the isolation of the substitution product $M\boldsymbol{L}$ and provides valuable information about the current efficiency for electrocatalysis, as shown in Table 1. Cyclic voltammetry of metal carbonyl solutions in the presence of added nucleophiles is a readily available technique for the expeditious study of the reactive intermediates involved in the electrocatalytic substitution of metal carbonyls, as listed in Table 2 and shown in Figs. 1–4. Coupled with the use of the Feldberg technique for the digital simulation of the cyclic voltammograms in Figs. 5 and 6, we have established the kinetics and mechanism of electrocatalysis for ligand substitution in considerable, quantitative detail. Two aspects of the electrocatalytic mechanism are of particular concern here, as they relate to (a) the lability of the 17-electron intermediate ML^+ and (b) the redox catalysis of added ligand $\boldsymbol{L}$.

Ligand substitution of ML^+

Previous studies have shown that the isomerizations of various Group VIB metal carbonyls can be catalyzed by anodic oxidation [23,30–32]. The isomerization step has been associated with 17-electron cation radicals, consistent with the view that the coordination shell of such transient intermediates is labile toward reorganization. Classic studies by Brown and coworkers have also revealed the substitution lability of neutral, odd-electron metal carbonyls in ligand exchange reactions proceeding via chain mechanisms [33–39]. The kinetics of ligand substitution in metal carbonyl radicals have recently been examined in two systems. McCullen, Walker and Brown [5] showed that the substitution of the phosphine ligand in the persistent $Mn(CO)_3(PR_3)_2$ by carbon monoxide proceeded by a second-order (i.e., S_N2) displacement process. Similarly, Trogler and Basolo [6] have reported the displacement of carbon monoxide from the coordinatively saturated, 17-electron $V(CO)_6$ by PPh_3 to proceed by similar kinetics. These results agree with our conclusion that the 17-electron species derived from the diamagnetic metal carbonyls in Table 2 undergo ligand exchange by an associative process [40]. The enhanced reactivity of these radical cations toward ligand substitution (with second-order rate constants which can easily exceed $10^5\ M^{-1}\ s^{-1}$) may arise from favorable charge transfer interactions between the electron-deficient metal center and the donor nucleophile. Such an associative pathway is to be contrasted with the mechanism commonly observed for

many 18-electron Group VIB metal carbonyls, in which dissociative, S_N1 processes usually dominate over the competing S_N2 processes. Ligand substitutions of metal carbonyls which are catalyzed by electrochemical reduction have also been recently described [41,42]. Such processes proceed via the initial formation of labile 19-electron radical anions, but experimental evidence has not yet been adduced as to whether associative or dissociative mechanisms are involved. The report [42] of the reduction-catalyzed substitution of the cationic $(phen)(CO)_3Re(NCMe)^+$ is particularly relevant to our studies with the neutral $(\eta^5\text{-}C_5H_5)Re(CO)_2(py)$ reported in Table 1. Apparently the rhenium(0) complex $(phen)(CO)_3Re(NCMe)$ and the rhenium(II) cation $(\eta^5\text{-}C_5H_5)Re(CO)_2(py)^+$ are the labile species responsible for ligand substitution.

Redox catalysis by added nucleophiles

Electrocatalytic studies reveal alternative routes by which added nucleophiles can participate in the ligand substitution of metal carbonyls. Thus phosphines such as $P(OMe)Ph_2$ and $PMePh_2$ are oxidized by radical-cation intermediates ML^+ in eqs. 15 and 16, respectively. The result leads to a "catalytic wave effect" in which characteristic distortions (elongation) of the cyclic voltammetric waves are observed, as found in Figs. 5(d), 6(b,c) and 8(b,c). The effect is described as redox catalysis, and it can be quantitatively analyzed by digital simulation of the cyclic voltammograms using the appropriate kinetic parameters for ligand substitution and electron transfer. Redox catalysis was also observed with other phosphines which qualitatively followed their donor abilities in the order: $PPh_3 < P(OPh)_3 < P(OMe)Ph_2 < P(p\text{-}MeC_6H_4)_3 < P(Me)Ph_2 < PEt_3$. Indeed this trend accords with the origin of redox catalysis from the rate of phosphine oxidation by electron transfer in eq. 18. It is important to emphasize however that the rate constant k_3 for eq. 18 is generally several orders of magnitude smaller than the rate constant k_2 for electron transfer from the metal carbonyl in eq. 13. Consequently, redox catalysis will only be observed in bulk electrolysis during the later stages of ligand substitution when the concentration of the reactant ML is severely diminished (i.e., $k_3[L] \gtrsim k_2[ML]$.) Since this kinetic situation also holds for the CV experiment, it follows that the reactant wave ML is minimally affected by the redox catalytic phenomenon, as elaborated in the discussion pertaining to Fig. 11 in the Experimental section.

An alternative process by which the radical cation of the metal cation of the metal carbonyls can react with the added nucleophile is shown in Fig. 10. In this system, the reversible cyclic voltammogram of the product ML is rendered irreversible by added nucleophile, owing to the effective interception of the radical cation ML^+ shown in Fig. 9. Indeed the enhanced nucleophilic reactivity of alkyl isocyanides generally causes such distortions in the CV waves of other metal carbonyls. Nonetheless the rates are not sufficient to affect adversely the efficiency of the electrocatalytic cycle listed in Table 1.

Experimental section

Materials

The substituted carbonylmanganese complexes, $(\eta^5\text{-}C_5H_4Me)Mn(CO)_2L$ listed in Table 2 were prepared from $(\eta^5\text{-}C_5H_4Me)Mn(CO)_2(THF)$, which was generated in situ by the irradiation of a solution of $(\eta^5\text{-}C_5H_4Me)Mn(CO)_3$ in THF under argon.

The photochemical reactor consisted of a 300 ml cylindrical flask with a 100 watt medium pressure Hg lamp contained in a quartz immersion well.

All preparative reactions and ligand exchange studies were carried out under either a nitrogen or an argon atmosphere. Benchtop manipulations were performed in Schlenk flasks. Many of the manganese complexes employed in this study are generally air sensitive, both in the solid state as well as in solutions. In a typical procedure, a solution of 2 g (η^5-C_5H_4Me)$Mn(CO)_3$ in 300 ml THF was deaerated, and irradiated for 50 min at 0°C. The IR spectrum of the solution indicated that ~ 90% of the starting material was converted to (η^5-C_5H_4Me)$Mn(CO)_2$(THF). One equivalent of the appropriate ligand (L = py, MeCN, PEt_3, $P(Me)Ph_2$, $P(OMe)Ph_2$, $CNCMe_3$, etc.) was added, and the solution stirred for several hours at ambient temperatures. During this period, the deep purple color of the THF complex gave way to the yellow or orange color of the product. The THF was removed at reduced pressure, and the residue was taken up in ethyl ether. (When the product was not soluble in ether, chloroform was employed.) Filtration of the solution, followed by crystallization from a mixture of ether and hexane or chloroform and ethanol afforded crystalline products in 30–70% yield. (η^5-C_5H_5)$Re(CO)_2$(py) [13] and (η^5-C_5H_5)$Re(CO)_2(PPh_3)$ [43] were synthesized from (η^5-C_5H_5)$Re(CO)_2(Et_2O)$ by thermal displacement of diethyl ether according to Giordano and Wrighton [13]. The preparations of *cis*-$(py)_2Mo(CO)_4$ [44], *cis*-$(t\text{-}BuNC)_2Mo(CO)_4$ [45], (η^5-C_5H_4Me)$Mn(CO)_2$(THF) [8] were carried out by the reported procedures. (η^5-C_5H_4Me)$Mn(CO)_3$ was obtained from Alfa/Ventron. Methyldiphenylphosphine was purchased from Organometallics, Inc. and methoxydiphenylphosphine was obtained from Arapahoe Chemicals. Triethylphosphine was obtained from Pressure Chemical Co. t-Butyl isocyanide was prepared by a literature method [46].

Reagent grade acetonitrile (Fisher Scientific) was further purified by distillation from calcium hydride, followed by stirring over a mixture of potassium permanganate and sodium carbonate for 24 h at room temperature. The acetonitrile was distilled at reduced pressure and then redistilled from phosphorous pentoxide. A final fractional distillation from calcium hydride through a 19-plate bubble cap (Oldershaw) column afforded acetonitrile suitable for electrochemistry. It was stored in a Schlenk flask under argon. For electrochemical use, tetrahydrofuran (THF) was distilled from lithium aluminum hydride, and stored under argon. For most of the preparative reactions, unpurified THF was adequate. Tetraethylammonium perchlorate (TEAP) and tetrabutylammonium perchlorate (TBAP) were used as received from G.F. Smith Chemical Co.

Electrochemical measurements

Electrochemistry was performed with a Princeton Applied Research Model 173 potentiostat equipped with a Model 176 current-to-voltage converter, which provided a feedback compensation for ohmic drop between the working and reference electrodes. The high impedance voltage follower amplifier (PAR Model 178) was mounted external to the potentiostat to minimize the length of the connection to the reference electrode for low noise pickup. Cyclic voltammetry was performed in a cell designed according to Van Duyne and Reilley [47]. The configuration of this cell is convenient for low temperature experiments since the lower portion of the cell containing the working solution could be easily submerged in the desired cold bath contained in a Dewar flask. The distance between the Pt electrode and the tip of the

salt bridge was less than 2 mm to minimize ohmic drop. The reference electrode was isolated from the cold bath and maintained at room temperature (~ 25°C). The voltammograms were recorded on a Houston Series 2000 X-Y recorder. Bulk electrolysis was performed in a 3-compartment cell equipped with a Pt-gauze working electrode and a magnetic stir bar for agitation. A sidearm provided an inlet for the inert atmosphere, and another permitted the removal of samples of solution. CV scans were recorded several minutes after agitation to ensure thermal equilibration. Electrode aging was not a serious problem in this study. Between experiments the platinum wire was soaked briefly in concentrated nitric acid, rinsed with distilled water, and dried at 110°C. The variation in effective electrode area from day to day was less than 10%.

For bulk electrolysis at a controlled potential, the current/time profile was stored in a Princeton Applied Research Model 4102 signal recorder for later output onto the X-Y recorder. Voltage/time profiles for electrolysis at a controlled current were recorded manually. For bulk electrolyses which required the intermittent sampling of the anolyte by cyclic voltammetry, a specially constructed cell incorporating an auxiliary Pt microelectrode was employed, as described in detail elsewhere [48].

Electrocatalysis of ligand exchange: typical example

The ligand substitution of (η^5-C_5H_4Me)$Mn(CO)_2$(NCMe) by t-butyl isocyanide is reported in detail as a typical example of the experiments listed in Table 1. A sample of (η^5-C_5H_4Me)$Mn(CO)_2$(NCMe) (110 mg, 0.48 mmol) was added to 12 ml of MeCN containing 0.1 *M* TEAP under a nitrogen atmosphere in the electrolysis cell. The stirred solution was reduced at −0.5 V vs. saturated NaCl SCE for several minutes to render harmless the traces of impurities which may have resulted from adventitious oxidation. When the cathodic current had fallen below about 10 μA, an aliquot of t-butyl isocyanide (40 mg, 0.48 mmol) was added with the aid of a microsyringe. The electrode potential was maintained at −0.5 V and the solution stirred at room temperature for 1 h in subdued roomlight. A 0.25 ml aliquot of the solution was removed and analyzed by IR spectrophotometry to verify that no reaction has occurred. The solution was then oxidized at a controlled current of 100 μA, and the electrode potential monitored. After 21.1 min the potential increased sharply from about 0.0 to +0.3 V, and the oxidation ceased. By this time, the deep yellow color of the starting solution had been replaced by the pale yellow color of the product. The carbonyl stretching frequencies in the IR spectrum of (η^5-C_5H_4Me)$Mn(CO)_2$(NCMe) shifted from 1932 and 1857 cm^{-1} to 1940 and 1881 cm^{-1}, which corresponded to that of the t-butyl isocyanide complex. The anolyte was transferred to a 25 ml volumetric flask and diluted to volume with a solution of deoxygenated MeCN containing 0.1 *M* TEAP. The yield of (η^5-C_5H_4Me)$Mn(CO)_2$-($CNCMe_3$) was determined by IR spectrophotometry to be 95 ± 7%, after correction for sampling. For calibration purposes, the product of the optical path length and the molar absorbtivity were evaluated using solutions of authentic (η^5-C_5H_4Me)$Mn(CO)_2$($CNCMe_3$) in MeCN containing 0.1 *M* TEAP. The plot of absorbance vs. concentration was linear in the concentration range of interest. The anolyte was diluted with 100 ml of deoxygenated water and the resulting light yellow precipitate isolated by filtration (94 mg, 72% isolated yield). The isolated product was found to be spectroscopically identical to that of authentic (η^5-C_5H_4Me)$Mn(CO)_2$($CNCMe_3$). The melting point of the sample after a recrystalliza-

tion from hexane was 52–54°C. Although the substitution products were not isolated in many of the other reactions listed in Table 1, they were positively identified by their IR spectra in the working solution by comparison with authentic samples.

Reaction of (η^5-C_5H_4Me)$Mn(CO)_2$[CNBu-t]$^+$ with t-butyl isocyanide

A solution of (η^5-C_5H_4Me)$Mn(CO)_2$(CNBu-t) (5.53×10^{-5} mol) in 15 ml of acetone containing 0.1 *M* TEAP was electrolyzed at a constant potenial of 1.0 V at −40°C. An excellent conversion to the radical cation was indicated with an initial negative scan cyclic voltammogram of the solution showing it to be identical with that shown in Fig. 9(a). Immediate addition of a 3-fold excess of t-butyl isocyanide afforded a solution which exhibited a single reversible CV was displaced to E^0 −0.03 V, and identical to S in Fig. 9. However, isolation of this species was impossible since it was thermally unstable and decomposed rapidly even at −20°C with concomitant disappearance of all electroactive material from the solution. The CV wave S was tentatively assigned to the disubstitution product (η^5-C_5H_4Me)-$Mn(CO)$[CNBu-t]$_2$ on the basis of the correlation of the value of E^0 −0.03 V with the trend established with other ligands [49]. This assignment is also consistent with the observation of the same CV wave when L = CO, PR_3 and $P(OR)_3$ were present in (η^5-C_5H_4Me)$Mn(CO)_2$L with t-butyl isocyanide.

Digital simulation of cyclic voltammograms for electrocatalytic ligand substitution

The computer program for the digital simulation of the cyclic voltammograms was written in Fortran, and is available upon request. It represents an adaptation of the subroutine package originally developed by Feldberg [14], and most of his nomenclature is preserved. The mechanism outlined in Scheme 1 or equivalently Scheme 1′ is the basis of the kinetic model of the ECE process for the catalytic ligand substitution under study. The heterogeneous rate constants for $\overline{Mn}$L (species 1) and $\overline{Mn}$***L*** (species 2) are represented as $k_s(1)$ and $k_s(2)$, respectively. The homogeneous rate constant for ligand exchange in the cation $\overline{Mn}L^+$ is k_1 (M^{-1} s^{-1}), and the electron transfer rate constant in eq. 13 is k_2. The required initial conditions are: $[(2)]_0 = 0$, $[(1)]_0 > 0$, $[\boldsymbol{L}]_0 > 0$. The other required inputs are self-explanatory since the program is written to be used interactively.

The simulated cyclic voltammograms are generated as 1000 current-voltage points which are stored in 2 data files, 50 and 51, respectively, in our code system (see statements 120–199). Although the output may be utilized in any number of ways, we found two particularly useful procedures: (1) the current-voltage points were plotted directly on to an X-Y recorder for visual presentation, and (2) the data were transferred to a Princeton Applied Research Model 4102 transient recorder and displayed on an oscilloscope. The latter method is useful for locating the exact magnitude of current maxima and minima since the transient recorder has a manual cursor and provides a digital readout of the desired data point.

The computer program also includes those electrocatalytic processes in which kinetic complications arise from the further reaction of the product radical cation ML^+ such as phosphine oxidation etc. The kinetic schemes for these processes are described individually below.

Redox catalysis involving the oxidation of $PMePh_2$

The increase of the anodic peak currents in Figs. 6(b) and 6(c) is not consistent

with a process involving the exchange of a single electron from $PMePh_2$, but two electrons. Accordingly, the following scheme was employed.

SCHEME 2′

$$MI \xrightarrow{k_3} ML^+ \tag{17}$$

$$ML^+ + PMePh_2 \underset{k_{-3}}{\overset{k_3}{\rightleftharpoons}} ML + PMePh_2{}^+ \tag{28}$$

$$PMePh_2{}^+ \xrightarrow{k_5} PPh_2{}^+ + Me\bullet \tag{29}$$

$$Me\bullet + ML^+ \rightarrow ML + Me_{ox} \tag{30}$$

and/or

$$Me\bullet + SH \rightarrow MeH + S\bullet \tag{31}$$

$$S\bullet + ML^+ \rightarrow ML + S_{ox} \tag{32}$$

where the subscript ox indicates a product of oxidation and SH represents the solvent. (Since the overall kinetics are not dependent on a knowledge of the fate of the methyl radical formed in eq. 29, two possibilities are presented in eq. 30 and eqs. 31, 32 [50].)

The CV behavior of the ML wave depends on the values of k_3, k_{-3} and k_5. However, two limiting kinetic situations can be considered with respect to the relative values of k_5 and k_{-3} [ML]. When $k_5 \gg k_{-3}$ [ML], the forward reaction in eq. 28 is rate-limiting, but when the converse is true, dissociation in eq. 29 is rate-limiting, and eq. 28 can be considered a pre-equilibrium. For a given concentration of ML, the relative anodic peak currents for the ML wave in the presence and absence of phosphine is given by the ratio i_p/i_p^0 at a constant v. The variation of this ratio with v, [ML] and [$PMePh_2$] allows a distinction to be made between these kinetically limiting situations, by the digital simulation procedure described by Saveant and coworkers [29]. Application of such a procedure to the oxidation of $PMePh_2$ by ML^+ indicates that k_3 is rate-limiting, with a rate constant of $1.5 \pm 0.5 \times 10^3\ M^{-1}\ s^{-1}$. We note that the agreement of the mechanism for the catalytic oxidation of $PMePh_2$ by ML^+ with that in Scheme 2′ applies to the timescale of the CV experiment. For longer times, as in the bulk electrolysis, this scheme does not appear to be valid since the slope of Fig. 7 corresponds to the partial stoichiometry:

$$ML^+ + 2\ PMePh_2 \rightarrow ML, \text{ etc.} \tag{33}$$

whereas the stoichiometry based on Scheme 2′ is

$$2\ ML^+ + PMePh_2 \rightarrow 2\ ML, \text{ etc.} \tag{33′}$$

The discrepancy may arise from the intervention of reactions following those included in Scheme 2′, and are sufficiently slow on the CV timescale so as not to perturb the voltammograms. The stoichiometry in eq. 33 is reminiscent of that for a polymerization process; indeed such processes have been previously described for the direct electrochemical oxidation of PPh_3 [51].

Electrocatalysis of ligand substitution coupled with redox catalysis

The digital simulation of the complete cyclic voltammogram of (η^5-C_5H_4Me)-

$Mn(CO)_2(py)$ in the presence of $PMePh_2$ in Fig. 8 requires a knowledge of the following parameters: E^0, β, and k_s for both $\overline{Mn}(py)$ and $\overline{Mn}(PMePh_2)$, as well as the values of the homogeneous rate constants k_1, k_2 and k_3. Values of E^0, β and k_s were determined independently from the cyclic voltammograms of the pure manganese carbonyls as: E^0 0.11 V, $\beta = 0.5$ and k_s 0.038 cm s^{-1} for $\overline{Mn}(py)$ and as E^0 0.48 V, $\beta = 0.5$ and k_s 0.034 cm s^{-1} for $\overline{Mn}(PMePh_2)$. Proceeding from these parameters, the value of k_3 $1.5 \pm 0.5 \times 10^3$ M^{-1} s^{-1} for eq. 28 was determined as described above. (For Fig. 6 and Fig. 8, we found that a value of k_3 1×10^3 M^{-1} s^{-1}, which is within the experimental error limits, provided a better fit of the computer simulated CV.) This value of k_3 is sufficiently small that the oxidation of $PMePh_2$ by eq. 28 can be neglected in comparison with the rate of electron transfer in eq. 21 for potentials of ~ 0.1 V. For example, consider the ratio $k_2[\overline{Mn}(py)]/k_3[PMePh_2]$. Since $k_2 \geqslant 10^5$ M^{-1} s^{-1} as described in ref. [8b] and the ratio $[\overline{Mn}(py)]/[PMePh_2] > 0.1$ in our experiments, the effect of eq. 28 is seen to contribute $< 10\%$ to the current of the $\overline{Mn}(py)$ wave. Thus the $\overline{Mn}(py)$ wave in the presence of $PMePh_2$ depends mainly on the values of k_1 and k_2. Figure 11 shows the variation of the ratio i_p/i_p^0 for this wave, as a function of the quantity log $([PMePh_2]RT/Jv)$, which is related to the effectiveness of ligand substitution. The theoretical curves obtained by digital simulation based on Scheme 1′ are drawn on the same figure (top scale) as the quantity log $(k_1[PMePh_2]RT/Fv)$. Curve a corresponds to the limit of $k_2 = 0$, whereas curve b represents the other limit of $k_2 = \infty$. It is seen that the value of k_2 has little influence within the precision of the experimental data. Comparison of the two scales in the abscissa leads to k_1 4×10^2 M^{-1} s^{-1}. We have thus shown that all the parameters required for the digital simulation of the cyclic voltammograms in Fig. 8 can be evaluated independently, with the exception of k_2. However this homogeneous rate constant has little effect on the voltammograms provided it is chosen sufficiently large (vide infra). For the simulations in Fig. 8, the value of k_2 2×10^5 M^{-1} s^{-1} was employed.

Redox catalysis involving the oxidation of $P(OMe)Ph_2$

The cyclic voltammogram in Fig. 5(d) can be treated by a kinetic scheme analogous to that presented above for $PMePh_2$. Similar to the fragmentation in eqs. 29–32, a methoxy group is cleaved from the radical cation $P(OMe)Ph_2^+$ leading to an overall two-electron process. As in the preceding system, the thermodynamic and kinetic parameters were evaluated independently from $\overline{Mn}(NCMe)$ and $\overline{Mn}$-$[P(OMe)Ph_2]$. Figures 5b and 5c show that phosphine oxidation is negligible at high scan rates and low phosphine concentrations. The values of the homogeneous rate constants can then be deduced as k_1 2.5×10^4 M^{-1} s^{-1} and k_2 2×10^5 M^{-1} s^{-1}, using the simulation technique described earlier [8]. The rate constant k_3 for the redox catalysis by phosphine oxidation in eq. 15 was the sole variable in Fig. 5d, and it was determined by the simulation procedure described above as 1×10^2 M^{-1} s^{-1}.

The effect of the electron transfer rate constant k_2 on the cyclic voltammograms

The magnitude of k_2 largely affects the relative contribution of the homogeneous (eq. 13) and heterogeneous (eq. 14) electron transfer processes to the reduction of the product cation-radical ML^+ in Scheme 1. It has little or no effect on the rate of ligand substitution which is governed solely by k_1. This kinetic description can be rationalized as follows: if k_2 is sufficiently large, the concentration of ML^+, which is

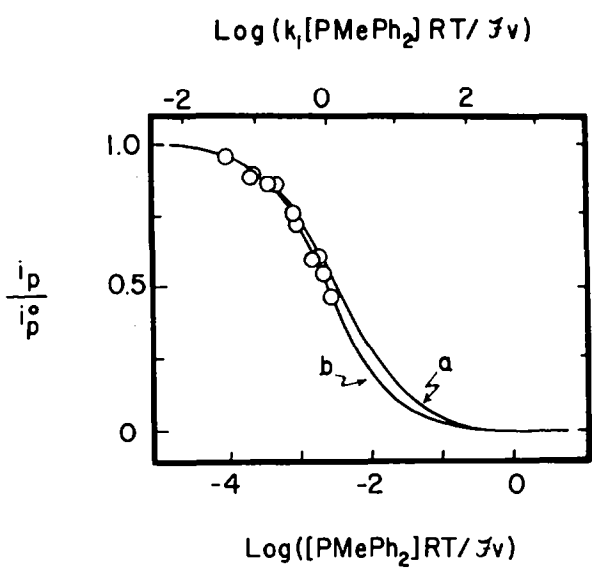

Fig. 11. Variations of the anodic peak current in the cyclic voltammogram of $(\eta^5\text{-}C_5H_4Me)Mn(CO)_2(py)$ in the presence (i_p) and the absence (i_p^0) of phosphine as a function of $\log([PMePh_2]RT/Fv)$, where v = scan rate and $[PMePh_2]$ = phosphine concentration. The lines are theoretical variations of the same peak current ratio drawn against $\log(k_1[PMePh_2]RT/Fv)$ at the limiting values for k_2 of (a) zero and (b) infinite.

produced at a rate controlled by eq. 12, will obey the steady state condition given by:

$$[ML^+] = [ML^+](k_1[L]/k_2[ML]) \tag{34}$$

On the other hand, if k_2 is small, $[ML^+]$ will suffer mainly a heterogeneous reduction at the electrode, and the rate-limiting step is still eq. 12, and in this case $[ML^+] \cong [ML^+]$ [52]. Thus eq. 12 is the rate determining step, independent of the exact value of k_2, which explains why it exerts little effect on the cyclic voltammogram. However a minor effect is noted when $k_2 \sim k_1$ in the following way. As seen above, when k_2 is large, $[ML^+]$ is given by eq. 34. As the value of k_2 decreases and approaches that of k_1, $[ML^+]$ will increase until it reaches its maximum value equal to $[ML^+]$. This situation is formally met when $k_2 = k_1[L]/[ML]$. We can thus conclude that for a given value of $k_1[L]/[ML]$ dictated by the particular system, the reduction of ML^+ occurs mainly in solution by eq. 13 when $k_2 > k_1[L]/[ML]$, whereas it will be reduced mainly at the electrode by eq. 14 in the reverse situation. At these kinetic extremes, the value of k_2 has no effect on the cyclic voltammograms, except a slight effect will be observed when $k_2 \cong k_1[L]/[ML]$ corresponding to a transition from one limiting situation to the other.

Acknowledgement

We wish to thank the National Science Foundation for financial support, the CNRS (France) and NSF for a joint fellowship to C.A., and Paul Zizelman for the synthesis of some of the metal carbonyls used in this study.

References

1 F. Basolo and R.G. Pearson, Mechanisms of Inorganic Reactions, 2nd Ed.; Wiley (Interscience): New York, 1967; p.533.
2 G.R. Dobson, Acc.Chem.Res., 9 (1976) 300.
3 A.J. Deeming, Inorganic Reaction Mechanism, Spec.Period.Report 7, 1981, 275 and related reviews in this series. D.J. Darensbourg, Adv. Organometal. Chem., 21 (1982) 113.
4 F.A. Cotton and G. Wilkinson, Advanced Inorganic Chemistry, 4th Ed.; Wiley, New York, 1981, p. 1185ff.
5 S.B. McCullen, H.W. Walker and T.L. Brown, J.Am.Chem.Soc., 104 (1982) 4007.
6 Q. Shi, T.G. Richmond, W.C. Trogler and F. Basolo, J.Am.Chem.Soc., 104 (1982) 4032.
7 J.W. Hershberger, R.J. Klingler and J.K. Kochi, J.Am.Chem.Soc., 104 (1982) 3034.
8 (a) J.W. Hershberger and J.K. Kochi, J.Chem.Soc.,Chem.Commun., (1982) 212;
(b) J.W. Hershberger, R.J. Klingler and J.K. Kochi, J.Am.Chem.Soc., in press.
9 G.L. Geoffroy and M.S. Wrighton, Organometallic Photochemistry, Academic Press, New York, 1979.
10 C.R. Bock and E.A. Koerner von Gustorf, Adv.Photochem., 10 (1977) 221.
11 M.S. Wrighton, Chem.Rev., 74 (1974) 401.
12 J. Nasielski, M. Vermeulen and P. Leepoel, J.Organometal.Chem., 102 (1975) 195.
13 P.J. Giordano and M.W. Wrighton, Inorg.Chem., 16 (1977) 160.
14 S.W. Feldberg, in A.J. Bard (Ed.), Electroanalytical Chemistry, Dekker, New York, 1969; Vol. 3, p. 199.
15 S.W. Feldberg in H.B. Mark (Ed.), Computer Applications in Analytical Chemistry, Dekker, New York, 1972, p. 185.
16 For the application of the digital simulation method to the study of other ECE substitution mechanisms, see refs. 17–21 and to isomerization reactions, see refs. 22 and 23.
17 (a) S.W. Feldberg and L. Jeftic, J.Phys.Chem., 75 (1971) 2381; (b) S.W. Feldberg and L. Jeftic, J.Phys.Chem., 76 (1972) 2439.
18 M.D. Hawley and S.W. Feldberg, J.Phys.Chem., 70 (1966) 3459.
19 J.M. Saveant, Accts.Chem.Res., 13 (1980) 323.
20 C. Amatore, J. Pinson, J.M. Saveant and A. Thiebault, J.Electroanal.Chem., 107 (1980) 59, 75.
21 (a) C. Amatore, J. Pinson, J.M. Saveant and A. Thiebault, J.Am.Chem.Soc., 103 (1981) 6930; (b) C. Amatore, J. Pinson, J.M. Saveant and A. Thiebault, J.Am.Chem.Soc., 104 (1982) 817.
22 S.F. Nelsen, E.L. Clennan and D.H. Evans, J.Am.Chem.Soc., 100 (1978) 4012.
23 A.M. Bond, D.J. Darensbourg, E. Mocellin and B.J. Stewart, J.Am.Chem.Soc., 103 (1981) 6827.
24 R.S. Nicholson, Anal.Chem., 37 (1965) 1351.
25 R.J. Klingler and J.K. Kochi, J.Phys.Chem., 85 (1981) 1731.
26 See discussion in ref. 8b.
27 R.S. Nicholson and I. Shain, Anal.Chem., 36 (1964) 706.
28 See Nicholson and Shain in ref. 27.
29 C.P. Andrieux, C. Blocman, J.M. Dumas-Bouchiat, F. M'Halla and J.M. Saveant, J.Am.Chem.Soc., 102 (1980) 3806, and references therein.
30 R.D. Rieke, H. Kojima and K. Ofele, J.Am.Chem.Soc., 98 (1976) 6735.
31 A.M. Bond, R. Colton and J. Jackowski, J.Inorg.Chem., 14 (1975) 274.
32 A.M. Bond, B.S. Grabaric and J. Jackowski, J.Inorg.Chem., 17 (1978) 2153.
33 D.R. Kidd and T.L. Brown, J.Am.Chem.Soc., 100 (1978) 4095.
34 B.H. Byers and T.L. Brown, J.Am.Chem.Soc., 99 (1977) 2527.
35 B.H. Byers and T.L. Brown, J.Am.Chem.Soc., 97 (1975) 947.
36 B.H. Byers and T.L. Brown, J.Organometal.Chem., 127 (1977) 181.
37 H.W. Hoffman and T.L. Brown, Inorg.Chem., 17 (1978) 613.
38 M. Absi-Halabi and T.L. Brown, J.Am.Chem.Soc., 99 (1977) 2982.
39 M. Absi-Halabi, J.D. Atwood, N.P. Forbus and T.L. Brown, J.Am.Chem.Soc., 102 (1980) 6248.
40 Note that the successful simulations of the cyclic voltammograms stem from the use of second-order kinetics for the ligand substitution step. See ref. 8.
41 G.J. Bezems, P.H. Rieger and S. Visco, J.Chem.Soc.Chem.Commun., (1981) 265.
42 D.P. Summers, J.C. Luong and M.S. Wrighton, J.Am.Chem.Soc., 103 (1981) 5238.
43 A.N. Nesmeyanov, N.E. Kolobova, Y.V. Makarov, B.V. Lokshin and E.B. Rusach, Izv.Akad.Nauk, SSSR,Ser.Khim, 3 (1976) 629.

44 R.E. Dessy and L. Wieczorek, J.Am.Chem.Soc., 91 (1969) 4963.
45 M.O. Albers and N.J. Coville, J. Organometal.Chem., 199 (1980) 55.
46 G.W. Gokel, R.P. Widera and W.P. Weber, Org.Syn., 55 (1976) 96.
47 R.P. Van Duyne and C.N. Reilley, Anal.Chem., 44 (1972) 142.
48 W. Lau, J.C. Huffman and J.K. Kochi, Organometallics, 1 (1982) 155.
49 See N.G. Connelly and M.D. Kitchen, J.Chem.Soc.,Dalton.Trans., (1977) 931 and ref. 7.
50 Cf. W.H. Tamblyn, R.J. Klingler, W.S. Hwang and J.K. Kochi, J.Am.Chem.Soc., 103 (1981) 3161.
51 G. Schiavon, S. Zecchin, G. Cogoni and G. Bontempelli, J.Electroanal.Chem., 48 (1973) 425.
52 C. Amatore and J.M. Saveant, J. Electroanal. Chem., 85 (1977) 27.